

# Numerical Renormalization Group Study of Probability Distributions for Local Fluctuations in the Anderson-Holstein and Holstein-Hubbard Models

Alex C. Hewson<sup>1</sup> and Johannes Bauer<sup>2</sup>

<sup>1</sup>Department of Mathematics, Imperial College, London SW7 2AZ, United Kingdom

<sup>2</sup>Max-Planck Institute for Solid State Research, Heisenbergstr.1, 70569 Stuttgart, Germany

**Abstract.** We show that information on the probability density of local fluctuations can be obtained from a numerical renormalisation group calculation of a reduced density matrix. We apply this approach to the Anderson-Holstein impurity model to calculate the ground state probability density  $\rho(x)$  for the displacement  $x$  of the local oscillator. From this density we can deduce an effective local potential for the oscillator and compare its form with that obtained from a semiclassical approximation as a function of the coupling strength. The method is extended to infinite dimensional Holstein-Hubbard model using dynamical mean field theory. We use this approach to compare the probability densities for the displacement of the local oscillator in the normal, antiferromagnetic and charge ordered phases.

## 1. Introduction

The numerical renormalization group [1, 2] (NRG) approach has been successfully applied to the calculation of static and dynamical response functions for models of magnetic impurities and quantum dots, and also been applied to lattice models, such as the Hubbard model, in the framework of dynamical mean field theory (DMFT) [3]. The response functions calculated give information about the low energy fluctuations which are of particular interest in the strong correlation regime. However, as a thermodynamic average is taken in calculating these response functions, some of the information about these fluctuations, which is contained in the original many-body states, is lost. Here we show that if we take only a partial thermodynamic average, such as in the calculation of a reduced density matrix, we can learn more about the nature of the local fluctuations, and how they vary as a function of the interaction terms.

We illustrate the approach first of all for the Anderson-Holstein impurity model. In the Anderson-Holstein model the occupation of the impurity state is linearly coupled to a local harmonic oscillator, which has spatial coordinate  $x$ , representing the lattice degrees of freedom around the impurity site. As the coupling of the oscillator to the impurity state is increased, the nature of the local fluctuations of the oscillator changes. If we take a full thermodynamic average then we only get averaged information about the oscillator. If we take a partial thermodynamic average, and calculate the reduced density matrix at the impurity site, treating the rest of the system as an 'environment', we can learn more about how the local lattice fluctuations vary as the coupling strength increases. From the reduced density matrix, calculated using the NRG, we can deduce the probability distribution  $\rho(x)$  for the  $x$  coordinate of the oscillator. From  $\rho(x)$  we can also deduce an effective potential  $V_{\text{eff}}(x)$ , and study the change of this potential as a function of the interaction strength and of the frequency of the local oscillator. Later in the paper, we extend the method to the infinite dimensional Holstein-Hubbard lattice model using dynamical mean field theory (DMFT) in combination with the NRG. We then compare how the local probability distribution  $\rho(x)$  changes in the normal, antiferromagnetic and charge ordered states for this model.

## 2. Local Fluctuations in the Anderson-Holstein Impurity Model

The Anderson-Holstein model corresponds to the single impurity Anderson model [4] with an additional linear coupling to a local phonon mode, as in the Holstein model [5]. The Hamiltonian takes the form,

$$\begin{aligned}
 H = & \sum_{\sigma} \varepsilon_f \hat{n}_{f,\sigma} + U \hat{n}_{f,\uparrow} \hat{n}_{f,\downarrow} + g(b^\dagger + b) \left( \sum_{\sigma} \hat{n}_{f,\sigma} - 1 \right) \\
 & + \sum_{\mathbf{k},\sigma} V_{\mathbf{k}} (c_{f,\sigma}^\dagger c_{\mathbf{k}\sigma} + \text{h.c.}) + \sum_{\mathbf{k}\sigma} \varepsilon_{\mathbf{k}} c_{\mathbf{k}\sigma}^\dagger c_{\mathbf{k}\sigma} + \omega_0 b^\dagger b.
 \end{aligned} \tag{1}$$

The impurity level  $\varepsilon_f$ , as in the usual Anderson model, is hybridised with conduction electrons of the host metal via a matrix element  $V_{\mathbf{k}}$ , with an interaction term  $U$  between

the electrons in the localized f (or d) state. There is in addition a coupling  $g$  of the impurity site occupation  $\hat{n}_{f,\sigma} = c_{f,\sigma}^\dagger c_{f,\sigma}$  to a local oscillator of frequency  $\omega_0$ . A measure of the hybridisation is the width factor,  $\Delta(\omega) = \pi \sum_{\mathbf{k}} V_{\mathbf{k}}^2 \delta(\omega - \varepsilon_{\mathbf{k}})$ , which for a flat conduction band of width  $W = 2D$ , and  $V_{\mathbf{k}}$  independent of  $\mathbf{k}$ , we can take as a constant  $\Delta = \pi V^2/2D$ . The oscillator coordinate operator  $\hat{x}$  in terms of the creation and annihilation operators,  $b^\dagger$  and  $b$ , is given by  $\hat{x} = (b + b^\dagger)/\sqrt{2\omega_0}$ , where we have taken the mass of the oscillator,  $M = 1$ . We have also set  $\hbar = 1$  so that  $x^{-1}$  has the dimension of square root of energy, and it is convenient to define characteristic length scale by  $x_0 = 1/\sqrt{\omega_0}$ . A convenient measure of the effects of the electron-phonon coupling on the electronic system is the parameter  $\lambda = 2g^2/\omega_0$ . In the limit  $\omega_0 \rightarrow \infty$ , such that  $\lambda$  remains finite, the model maps into the Anderson model with  $U \rightarrow U - \lambda$ ,  $\varepsilon_f \rightarrow \varepsilon_f + \lambda/2$ . The behaviour of the model has been studied using the NRG [6] and it has been used to study the transport through a quantum dot in the presence of a coupling of the occupation dot to local phonon modes [7].

To learn more about the state of the oscillator we use the NRG to calculate the reduced density matrix  $\rho_{\text{red}}$  at the impurity site. A procedure for calculating the reduced density matrix was introduced into NRG calculations by Hofstetter [8]. The original motivation was to find an improved way of calculating the higher energy features in the spectral density of the impurity Green's function in cases of broken symmetry. For NRG calculations the system is recast in the form of a linear chain with impurity at one end. Sequential diagonalisations are then carried out starting at the impurity site. The information from the shorter length chains is used to calculate the higher energy features in the spectral density, and the longer chains the low energy features. In the case of broken symmetry the ground state for the shorter chains underestimates the degree of symmetry breaking. In Hofstetter's modified procedure the ground state is first estimated from the longest chain calculated, and then used to deduce the density matrix of the sites corresponding to shorter chain lengths. Incorporating the reduced density matrix into the calculation of the spectral density from the shorter chains corrects the deficiencies of the standard approach in the case of broken symmetry. Refinements of this approach have been introduced more recently based on the use of a complete set of NRG states [9, 10]. These have the advantage that the sum rules on the total spectral density are satisfied exactly, rather than approximately as in earlier versions of the NRG approach.

The calculation of the density matrix gives additional information which we can exploit. For example in the Anderson-Holstein model, if we work backwards from the longest chain, we can deduce the reduced density matrix at the impurity site  $\rho_{f,\text{red}}$ . The matrix elements of this reduced density matrix will be with respect to the basis states at the impurity site, the states of all the other sites are averaged over as they are taken to be part of the environment. The electronic states at the impurity site can be labeled by the local charge  $q$  ( $q = \sum_{\sigma} n_{f,\sigma}$ ), and the  $z$ -component of spin  $m_z$ , and the index of the harmonic oscillator states  $\nu$ . The matrix will be diagonal with respect to the spin and charge indices, and so a typical matrix element can be expressed as  $(\rho_{f,\text{red}}(q, m_z))_{\nu,\nu'}$ .

The probability distribution function  $\rho(x)$  for the oscillator coordinate  $x$  is given by

$$\rho(x) = \sum_{q, m_z} \rho(x : q, m_z) \quad (2)$$

where

$$\rho(x : q, m_z) = \sum_{\nu, \nu'} \phi_\nu(x) (\rho_{f, \text{red}}(q, m_z))_{\nu, \nu'} \phi_{\nu'}^*(x), \quad (3)$$

and  $\phi_\nu(x)$  is the normalised real space harmonic oscillator wavefunction,

$$\phi_\nu(x) = \left( \frac{\sqrt{\omega_0}}{\sqrt{\pi} 2^\nu \nu!} \right)^{1/2} e^{-\omega_0 x^2 / 2} H_\nu(\sqrt{\omega_0} x), \quad (4)$$

with the Hermite polynomial  $H_\nu(x)$  of order  $\nu$ .

It is possible to define an effective potential for the oscillator using an effective wavefunction defined by  $\psi_{\text{eff}}(x) = \sqrt{\rho(x)}$ , which is taken to be a solution of the one-dimensional Schrödinger equation (recall  $M = 1$ ,  $\hbar = 1$ ),

$$-\frac{1}{2} \frac{d^2 \psi_{\text{eff}}(x)}{dx^2} + V_{\text{eff}}(x) \psi_{\text{eff}}(x) = E \psi_{\text{eff}}(x), \quad (5)$$

or

$$V_{\text{eff}}(x) = E + \frac{1}{2} \frac{\psi_{\text{eff}}''(x)}{\psi_{\text{eff}}(x)}. \quad (6)$$

In terms of  $\rho(x)$  this translates into

$$V_{\text{eff}}(x) = E + \frac{1}{4} \left[ \frac{\rho''(x)}{\rho(x)} - \frac{1}{2} \left( \frac{\rho'(x)}{\rho(x)} \right)^2 \right]. \quad (7)$$

By construction this potential is such that the ground state wavefunction can be used to reproduce the NRG derived  $\rho(x)$ .

### 2.1. Results for the symmetric model

Unless otherwise stated we use in the following the parameters  $W = 2D = 2$ ,  $\pi\Delta = 0.1$  and  $\omega_0 = 0.1$  setting the energy scales for electrons and phonons in this section. The phonon frequency  $\omega_0$  has been chosen so that  $1/\omega_0$  is on the scale of the life time of a electron on the impurity site,  $\omega_0 \sim \pi\Delta$ . We know in the adiabatic limit  $\omega_0 \ll \pi\Delta$ , the  $x$  coordinate becomes a classical variable, and in the opposite limit  $\omega_0 \rightarrow \infty$  it maps on to an effective Hubbard model, so the range  $\omega_0 \sim \pi\Delta$  is the interesting one to investigate.

In Fig. 1 we give results for the probability distribution function  $\rho(x)$  for the symmetric model calculated as outlined above.

The results on the left hand panel correspond to  $U = 0$  ( $\varepsilon_d = 0$ ). We take as a relative measure of the strength of the phonon coupling and hybridisation scale the dimensionless factor  $\alpha = \lambda/\pi\Delta$  ranging from weak ( $\alpha \ll 1$ ) to strong coupling ( $\alpha \gg 1$ ). As  $\alpha$  increases the distribution broadens, and for  $\alpha = 1.5$  a two peak structure can be seen which becomes more marked as the coupling strength is increased further.

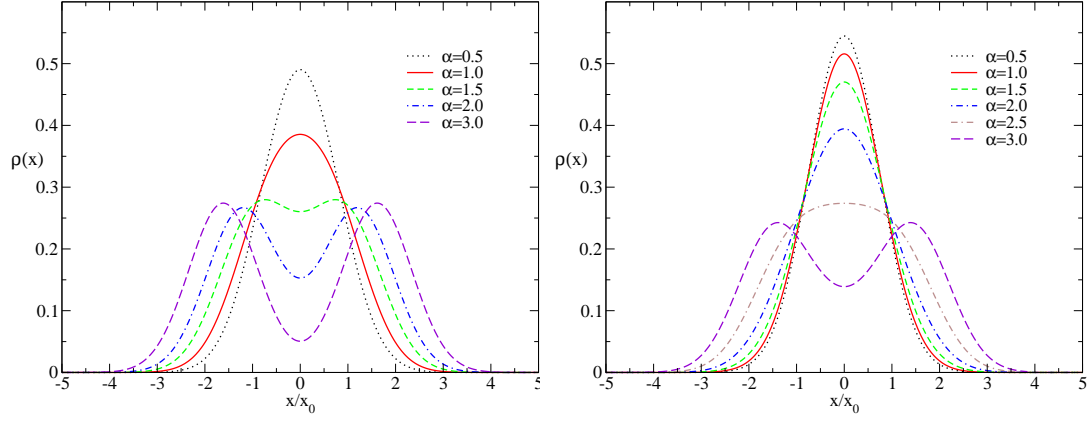


**Figure 1.** The total probability distribution function  $\rho(x)$  for the oscillator displacement  $x$  in the ground state for a range of values of  $\alpha$ , in the left panel with  $U = 0$  and the right with  $U/\pi\Delta = 2$ .

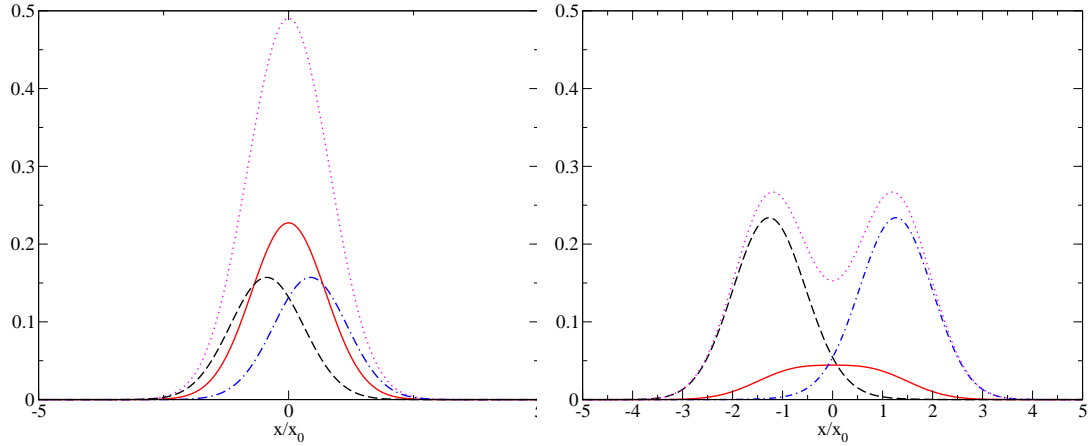


**Figure 2.** The components,  $\rho(x : 0, 0)$  (dot-dashed curve),  $\rho(x : 1, 1/2) + \rho(x : 1, -1/2)$  (full curve) and  $\rho(x : 2, 0)$  (dashed) of  $\rho(x)$  (dots) for the case  $\alpha = 0.5$  (left panel), and  $\alpha = 2.0$  (right panel) for  $U = 0$ .

In Fig. 2 we plot the individual components of  $\rho(x)$ ;  $\rho(x : 0, 0)$ ,  $\sum_{\pm} \rho(x : 1, \pm 1/2)$  and  $\rho(x : 2, 0)$ , corresponding to  $q = 0, 1, 2$ , for  $U = 0$ , for the two cases  $\alpha = 0.5$  (left panel) and  $\alpha = 2$  (right panel). One can see from these curves the two factors that lead to the two peak structure on increasing  $\alpha$ . One factor is that the maxima of curves corresponding to  $q = 0$  and  $q = 2$  are shifted on either side of central peak corresponding to  $q = 1$ . This reflects that fact that in these charge states for an isolated impurity the oscillator is displaced from  $x = 0$  to  $\sqrt{\lambda}/\omega_0$  and  $-\sqrt{\lambda}/\omega_0$  respectively. The other factor is that the weights of the peaks at  $q = 0$  and  $q = 2$ , compared to the weight of the central peak corresponding to  $q = 1$ , increases with  $\alpha$ . The integrated weight under the curve  $P_q$  is a measure of the probability of the occupation of the local level in the state with charge quantum number  $q$ . This shift in relative weights is due to the

fact that the coupling to the phonon mode induces a local attraction. The weight  $P_2$  measures the probability of the local level being doubly occupied which is equal to the expectation value  $\langle n_{f,\uparrow} n_{f,\downarrow} \rangle$ . For  $\alpha = 2$ , the weights  $P_0 = P_2 = 0.430261$  are in precise six figure agreement with  $\langle n_{f,\uparrow} n_{f,\downarrow} \rangle$  as calculated directly from the NRG calculation, and we have  $P_1 = 1 - P_0 - P_2 = 0.139478$ . Notice that for  $\alpha = 0$  the corresponding values are  $P_0 = P_2 = 0.25$ ,  $P_1 = 0.5$ . The relative shift of the weights can be explained to a large extent, but not completely, by the local induced attractive interaction. If we take a model with a local attractive interaction  $U/\pi\Delta = -2$ , but no phonon coupling, then the values deduced from the NRG for  $P_q$  are  $P_0 = P_2 = 0.38289$ ,  $P_1 = 0.23422$ , which underestimates the relative shift away from the state  $q = 1$  found in the phonon coupled model with  $\alpha = 2$ . This shows that the energetic gain of creating zero and doubly occupied sites is higher in the system with phonons as compared to the case with instantaneous attraction.

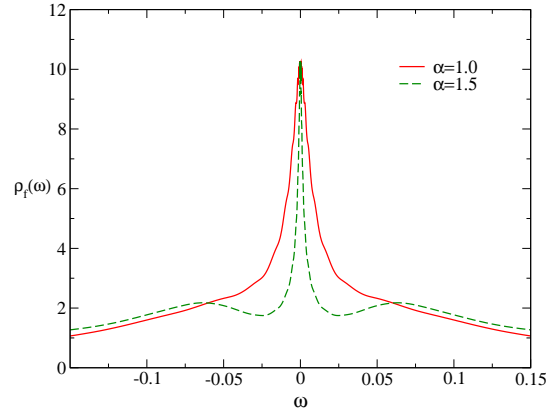


**Figure 3.** The spectral density  $\rho_f(\omega)$  for the impurity single electron Green's function for  $U = 0$  and  $\alpha = 1, 1.5$ .

The spectral density for the local f-electron Green's function  $\rho_f(\omega)$  is shown in Fig. 3 for  $U = 0$  for  $\alpha = 1$  and  $\alpha = 1.5$ . It can be seen that the development of the two peak form in  $\rho(x)$  correlates with the development of three peaks in  $\rho_f(\omega)$ . Clear shoulders can be seen in the result for  $\rho_f(\omega)$  for  $\alpha = 1$ , and the three peak form has fully emerged for  $\alpha = 1.5$ . The central peak becomes extremely narrow for values of  $\alpha$  in the strong coupling regime [6].

The effect of the interaction  $U$  in suppressing the onset of the double peak distribution can be seen by comparing the  $U = 0$  results with those shown in the right panel of Fig. 1 which are for the case  $U/\pi\Delta = 2$  ( $\varepsilon_f = -U/2$ ). The double peak structure, which develops in the  $U = 0$  case for  $\alpha \sim 1.5$ , develops in the  $U/\pi\Delta = 2$  case only when  $\alpha \sim 2.5$ . This is a smaller value than what is expected naively in the  $\omega_0 \rightarrow \infty$  case where  $U_{\text{eff}} = U - \lambda$  signaling again that for finite  $\omega_0$  when phonons can be excited the occupation of the zero and doubly occupied sites is energetically more favourable.

The corresponding effective potentials  $V_{\text{eff}}(x)$  for the  $U = 0$  case, as deduced from

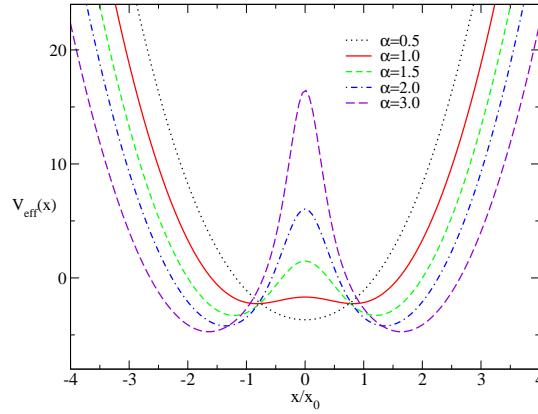


**Figure 4.** The effective potential  $V_{\text{eff}}(x)$  for  $U = 0$  and a range of values of  $\alpha$ , corresponding to the results for  $\rho(x)$  in the left panel of figure 1.

equation (7), are shown in Fig. 4. The on-set of a double well feature can be seen in the results for  $\alpha = 1.0$ , which is before a double peak structure can be seen in the corresponding  $\rho(x)$ . The effective potentials for higher values of  $\alpha$  have a clear double well form.

It is of interest to compare this potential with one calculated using a semiclassical approximation, in which we neglect the kinetic energy of the oscillator and treat the coordinate  $x$  as a classical variable. This is a commonly used approximation in taking the electron-phonon coupling into account, and corresponds to the Born-Oppenheimer approximation. Evaluating the impurity contribution to the total ground state energy  $E(x)$  as a function of  $x$  one arrives at an expression for the effective semiclassical potential,  $V_{\text{s-cl}}(x)$  ( $= E(x)$ ) given by

$$V_{\text{s-cl}}(x) = \varepsilon_f - \frac{2\Delta}{\pi} + \frac{\omega_0^2 x^2}{2} - \frac{2\bar{\varepsilon}_f(x)}{\pi} \tan^{-1}\left(\frac{\bar{\varepsilon}_f(x)}{\Delta}\right) + \frac{\Delta}{\pi} \log\left(\frac{\bar{\varepsilon}_f^2(x) + \Delta^2}{D^2}\right), \quad (8)$$

where  $\bar{\varepsilon}_f(x) = \varepsilon_f + \sqrt{2\omega_0 g}x$ .

In Fig. 5 we compare the semiclassical potential  $V_{\text{s-cl}}(x)$  with  $V_{\text{eff}}(x)$  deduced from equation (7) for  $\alpha = 1$  and  $\alpha = 2$ .

The relevant comparison is in the shapes of these potentials, not their absolute values, and they have been subject to a constant shift so their forms can be compared more easily. It can be seen that the potentials develop in a similar way as the coupling strength is increased, though when the double well form develops the potential barrier between the wells is less marked in the semiclassical case. The minima occur at very similar  $x/x_0$ -values;  $-0.74$  ( $V_{\text{s-cl}}(x)$ ) and  $-0.79$  ( $V_{\text{eff}}(x)$ ) for  $\alpha = 1$ , and  $-1.26$  ( $V_{\text{s-cl}}(x)$ ) and  $-1.35$  ( $V_{\text{eff}}(x)$ ) for  $\alpha = 2$ .

The coefficient of the  $x^2$  term in  $V_{\text{s-cl}}(x)$  changes sign for  $\alpha = 0.5$ , which is the point at which the double well begins to form. For  $\alpha > 0.5$  there are two mean field solutions for the expectation value  $\langle \hat{x} \rangle$  corresponding to the two minima in  $V_{\text{s-cl}}(x)$  and the local symmetry is broken. The positions of the minima in  $V_{\text{s-cl}}(x)$  can be deduced

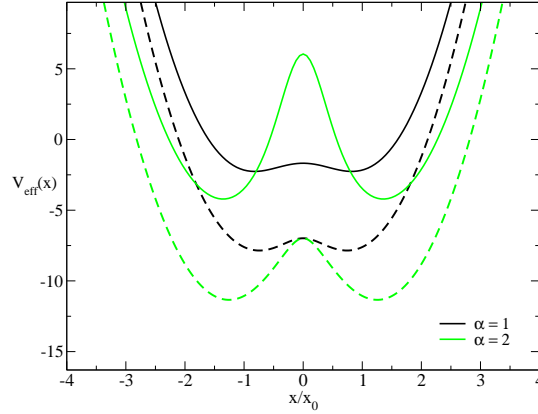


**Figure 5.** The effective potentials  $V_{\text{eff}}(x)$  (full lines) as deduced from equation (7), compared with corresponding the semiclassical potentials  $V_{\text{s-cl}}(x)$  (dashed lines), Eq. (8), for  $U = 0$ .

from the equation,

$$\frac{\partial V_{\text{s-cl}}(x)}{\partial x} = 0 = \omega_0^2 x + \sqrt{2\omega_0} g(n_f - 1), \quad (9)$$

where  $n_f$  is the mean field occupation value given by

$$n_f = 1 - \frac{2}{\pi} \tan^{-1} \left( \frac{\bar{\varepsilon}_f(x)}{\Delta} \right), \quad (10)$$

yielding

$$x = \langle \hat{x} \rangle_{\text{MF}} = -\frac{\sqrt{\lambda}}{\omega_0} (n_f - 1). \quad (11)$$

We can deduce an exact relation of this type by introducing an additional to term of the form  $c(b + b^\dagger)$  into the Hamiltonian. The ground state energy  $E(c)$  will be a function of the coupling  $c$  introduced, and we can deduce that

$$\left. \frac{\partial E(c)}{\partial c} \right|_{c=0} = \langle b + b^\dagger \rangle = \sqrt{2\omega_0} \langle \hat{x} \rangle. \quad (12)$$

If we now perform a canonical transformation  $H' = \hat{U}^{-1} H \hat{U}$  with  $\hat{U} = e^{-c(b^\dagger - b)/\omega_0}$ , the terms in  $H'$  which depend on  $c$  are

$$-\frac{c^2}{\omega_0} - \frac{2gc}{\omega_0} (\langle \hat{n}_f \rangle - 1). \quad (13)$$

As the canonical transformation does not effect the energy values we can use this result in equation (12) to determine  $\langle b + b^\dagger \rangle$ , which leads to the result,

$$\langle \hat{x} \rangle = -\frac{\sqrt{\lambda}}{\omega_0} (\langle \hat{n}_f \rangle - 1). \quad (14)$$

This is the same formula as derived from the semi-classical approximation as given in equation (11), except that the mean field value  $n_f$  is replaced by the exact value  $\langle \hat{n}_f \rangle$  for the impurity occupation. This result holds for  $U \neq 0$  and is exact.



In the mean field broken symmetry solutions we have the two broken symmetry solutions at strong coupling, such that  $n_f \sim 0$  and  $n_f \sim 2$ , giving from equation (11)  $\langle \hat{x} \rangle_{\text{MF}} \sim \pm \sqrt{\lambda}/\omega_0$  for the positions of the two minima  $V_{\text{s-cl}}(x)$ . In the exact solution for the impurity model, however, this broken symmetry must be restored and the average value of  $x$  must be zero. This is clearly the case in the NRG solution as  $\langle \hat{x} \rangle$  can be deduced from  $\rho(x)$ , using  $\langle \hat{x} \rangle = \int_{-\infty}^{\infty} x \rho(x) dx$ , and is zero as  $\rho(x)$  is symmetric. However we have seen that the positions of the minima in both  $V_{\text{eff}}(x)$  and  $V_{\text{s-cl}}(x)$  are very close so the mean field values for  $\langle \hat{x} \rangle_{\text{MF}}$  provide an estimate of the positions of the minima in  $V_{\text{eff}}(x)$ .

As  $\langle \hat{x} \rangle = 0$  in the exact solution for the symmetric model, a more interesting quantity to calculate is the root mean square deviation  $\Delta x$ , where  $(\Delta x)^2 = \langle (\hat{x} - \langle \hat{x} \rangle)^2 \rangle$ . In Fig. 6 we give a plot of  $\Delta x$  deduced from  $\rho(x)$  for the model with  $U = 0$  and several values of  $\alpha$ .

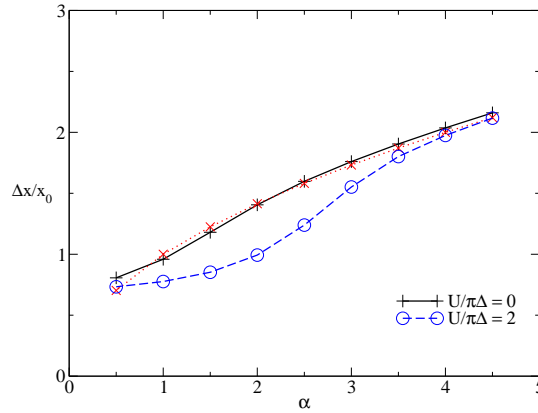


**Figure 6.** The root mean deviation  $\Delta x/x_0$  as a function of  $\alpha$  for the case  $U = 0$ ,  $\varepsilon_f = 0$  (full curve), and  $U/\pi\Delta = 2$ ,  $\varepsilon_f = -U/2$  (dashed curve). The dotted curve corresponds to  $\sqrt{\alpha \pi \Delta}/\omega_0$ .

It can be seen that  $\Delta x$  does vary significantly with  $\alpha$  reflecting the fact that in the strong coupling regime the deviation  $\Delta x$  is determined by position of the minima in the double potential wells. As the mean field values  $\langle \hat{x} \rangle_{\text{MF}}$ , were found to give a good estimate of these, and in the strong coupling regime  $\langle \hat{x} \rangle_{\text{MF}} \sim \pm \sqrt{\alpha \pi \Delta}/\omega_0$ , we compare in Fig. 6 this estimate with the calculated value of  $\Delta x$ . It is seen to provide a good estimate of  $\Delta x$  over the range of  $\alpha$  shown. Also in Fig 6 we give the values of  $\Delta x$  for the symmetric model with  $U/\pi\Delta = 2$ . The tendency for the  $U$  term to suppress the fluctuations for the lower values of the coupling strength  $\lambda$ , noted in Fig. 1, is apparent but to have only a relatively minor effect in the stronger coupling range.

## 2.2. Results for the asymmetric model

With only a small degree of asymmetry, the form for  $\rho(x)$  changes quite dramatically in the strong interaction regime. This is because the doubly occupied impurity state is now

predominantly favoured. In Fig. 7 we show results for  $\rho(x)$  in a case with  $\varepsilon_f/\pi\Delta = -0.5$  and  $U = 0$  for the same range of values of  $\alpha$  as in Fig. 1.

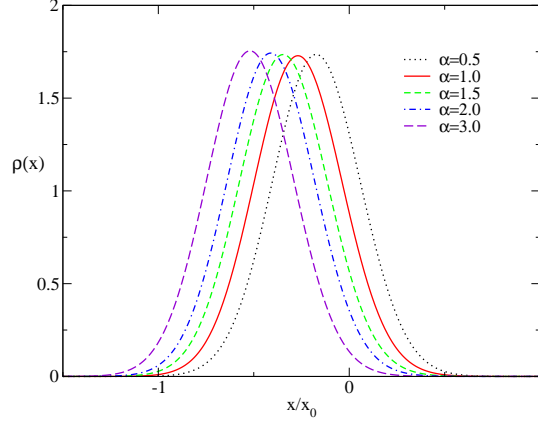


**Figure 7.** The total probability distribution function  $\rho(x)$  for the oscillator displacement  $x$  in the ground state for a range of values of  $\alpha$  with  $U = 0$  and  $\varepsilon_f/\pi\Delta = -0.5$ .

There is just a single narrow peak for  $\rho(x)$  in each case which shifts to slightly more negative values of  $x$  as  $\alpha$  increases. In Fig. 8 we compare the semiclassical potential and  $V_{\text{eff}}(x)$  as derived from equation (7) for the case  $\alpha = 1$ .

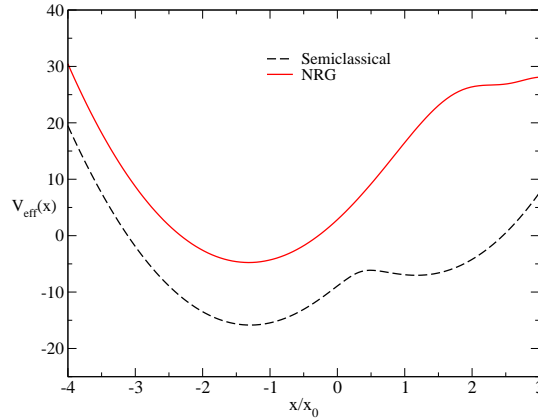


**Figure 8.** The effective potentials  $V_{\text{eff}}(x)$  (full curve) as deduced from equation (7), compared with corresponding the semiclassical potentials  $V_{\text{s-cl}}(x)$  (dashed curve) for  $\alpha = 2.0$ ,  $\varepsilon_f/\pi\Delta = -0.5$  and  $U = 0$ .

Both potentials have an absolute minimum at  $x/x_0 = -1.29$  though in the semiclassical case there is a secondary local minimum. This value of  $x/x_0$  agrees with that predicted by equation (14) using the value derived from  $\langle \hat{n}_f \rangle$  derived from the NRG calculation which gives  $x/x_0 = -1.2909$ . We can check the relation (14) by taking the average of  $x$  over the distribution  $\rho(x)$  and then compare with the result from equation (14) using

the NRG calculated  $\langle \hat{n}_f \rangle$ . The results for a range of values of  $\alpha$  are shown as points (crosses and plus signs) in Fig. 9 (smaller values for  $U = 0$ ,  $\varepsilon_f/\pi\Delta = -0.5$ , and larger values  $U/\pi\Delta = 2$ ,  $\varepsilon_f = -U/2 - 0.05$ ).

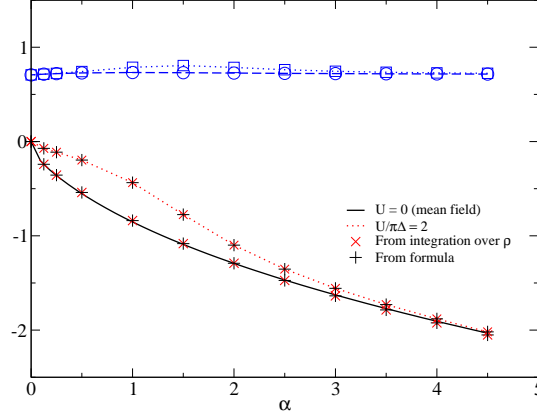


**Figure 9.** The values of  $\langle \hat{x} \rangle / x_0$  for  $U = 0$ ,  $\varepsilon_f/\pi\Delta = -0.5$ , and  $U/\pi\Delta = 2$ ,  $\varepsilon_f = -U/2 - 0.05$ , as calculated from the average of  $\rho(x)$  (crosses) and those deduced from equation (14) (plus signs). The mean field results for  $U = 0$  correspond to the full curve. The corresponding results for the root mean deviation  $\Delta x / x_0$  are also shown, for the case  $U = 0$ ,  $\varepsilon_f/\pi\Delta = -0.5$ , (dashed curve and circles), and  $U/\pi\Delta = 2$ ,  $\varepsilon_f = -U/2$  (dotted curve and squares).

For both sets of parameters, the results of the two calculations are in remarkably good agreement, giving the same values to at least five significant figures in all cases. The full curve in Fig. 9 corresponds to the mean field result ( $U = 0$ ) for  $\langle \hat{x} \rangle / x_0$  and can be seen also to be in good agreement with the exact results. Also shown in Fig. 9 is the root mean square  $\Delta x$  calculated from  $\rho(x)$ . Though the average displacement  $\langle \hat{x} \rangle$  increases with increasing  $\alpha$  it can be seen that  $\Delta x$  remains almost constant. In mean field theory  $\Delta x = 0$ , as in this approximation  $\langle \hat{x}^2 \rangle = \langle \hat{x} \rangle^2$ . In the semiclassical approach one could estimate  $\rho(x)$  by solving the Schrödinger equation (5) with the potential  $V_{s-cl}(x)$  and using  $\rho(x) = |\psi_{gs}(x)|^2$ , where  $\psi_{gs}(x)$  is the ground state wavefunction, and then use the result to take an average of  $x^2$ . We can, however, calculate it exactly in the limit of very weak and strong coupling limits. In the uncoupled case using the ground state wave function for the oscillator we find  $(\Delta x)^2 / x_0^2 = 1/2$ . In the strong coupling case with asymmetry we can take  $\langle \hat{n}_f \rangle = 2$  or  $\langle \hat{n}_f \rangle = 0$ , and use a displaced oscillator transformation to new phonon creation and annihilation operators,  $a^\dagger, a^{(\dagger)} = b^{(\dagger)} \pm g/\omega_0$ . The ground state  $|gs\rangle$  then corresponds to the state  $a|gs\rangle = 0$ , and in this state  $\langle b^\dagger b \rangle = g^2/\omega_0^2$ ,  $\langle \hat{x}^2 \rangle = x_0^2(1 + 4g^2/\omega_0^2)/2$ . We have from equation (14) with  $\langle (\hat{n}_f - 1) \rangle = \pm 1$ ,  $\langle x \rangle^2 = 2g^2 x_0^2 / \omega_0^2$ , which gives again  $(\Delta x)^2 / x_0^2 = 1/2$ , so that we find  $\Delta x / x_0 = 1/\sqrt{2}$  in both limits. This agrees well with the results shown in Fig. 9 and  $\Delta x$  does not deviate much from this value over the whole range of  $\alpha$ . As will be seen in the Sec. 3 for the case of the lattice model, the results will be different for  $\Delta x$  near the transition to a charge ordered state.

The corresponding values for the case with  $U/\pi\Delta = 2$ ,  $\varepsilon_f/\pi\Delta = -0.15$  are shown in the same Fig. 9. The effect of finite  $U$  is to suppress the value of  $\langle\hat{x}\rangle$  for smaller values of  $\alpha$ , but only has a marginal effect for  $\alpha \geq 3$  and has very little effect on  $\Delta x$ . Again there is five figure agreement in the the two calculations for  $\langle\hat{x}\rangle$ ; the one based on integrating over  $\rho(x)$  and the one using Eq. (14).

As the model in the limit  $\omega_0 \rightarrow \infty$  ( $\lambda$  finite) corresponds to an Anderson model with an interaction term  $U - \lambda$ . For  $U = 0$  and finite  $\lambda$ , therefore, it becomes equivalent to a negative- $U$  Anderson model. The symmetric model in the regime  $\lambda/\pi\Delta \gg 1$  has a Kondo effect due to charge rather than spin fluctuations. Introducing some asymmetry by changing  $\varepsilon_f$  from the value for the symmetric case is equivalent to introducing a magnetic field in the Kondo case [11], which for large fields suppresses the Kondo effect. We found that in using a value  $\varepsilon_f/\pi\Delta = -0.5$  that the mean field estimate for  $\langle\hat{x}\rangle$  and the exact result were in good agreement. This is due to the fact that this degree of asymmetry corresponds to the Kondo case with a large magnetic field, and also because the value of  $\omega_0$  used is much smaller than the bandwidth  $D$ . For a much smaller degree of asymmetry, which would correspond to a smaller 'magnetic' field, we should expect to find some limitations in the predictions from the semiclassical approximation. To examine this further we consider the case with  $\alpha = 2$  and  $\varepsilon_f/\pi\Delta = -0.01$ . In Fig. 10 we show the semiclassical potential and  $V_{\text{eff}}(x)$  derived from (7).

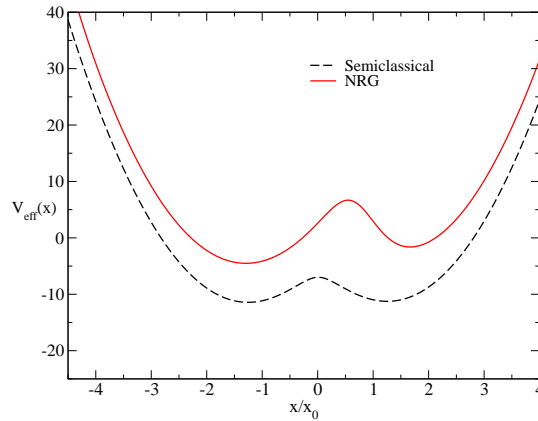


**Figure 10.** The effective potentials  $V_{\text{eff}}(x)$  (full curve) as deduced from equation (7), compared with corresponding the semiclassical potentials  $V_{\text{s-cl}}(x)$  (dashed curve) for  $\alpha = 2.0$ ,  $\varepsilon_f/\pi\Delta = -0.01$  and  $U = 0$ .

In this case we see that both potentials have two local minima. The absolute minimum in the two cases coincide at a value of  $x/x_0 = -1.26$ , which corresponds to the mean field estimate of  $\langle\hat{x}\rangle/x_0$ . The value obtained by averaging  $x$  over the distribution  $\rho(x)$ , and from the formula (14) with the NRG value for  $\langle\hat{n}_f\rangle$ , both give  $\langle\hat{x}\rangle/x_0 = -1.09888$ . The average value in this case no longer coincides with the absolute minimum of the potential as the fluctuations to the local neighbouring minimum make a significant contribution. As the semiclassical equation (11) for  $\langle\hat{x}\rangle$  agrees with the exact one in equation (14), this difference arises from the fact that the semiclassical prediction for  $n_f$  disagrees with

the exact value of  $\langle \hat{n}_f \rangle$ . The semiclassical prediction gives  $n_f = 1.889$  and the exact value from the NRG gives  $\langle \hat{n}_f \rangle = 1.777$ , which explains the difference in the predictions. It is interesting to note, however, that the semiclassical prediction does coincide with the absolute minimum of the effective potential derived from the NRG results.

The deviations from mean field theory become more marked for higher oscillator frequencies. In Fig. 11 we give a plot of  $\langle x \rangle/x_0$  for the case  $U = 0$  and  $\varepsilon_f/\pi\Delta = -0.1$  taking the phonon frequency value  $\omega_0 = 0.6$ .

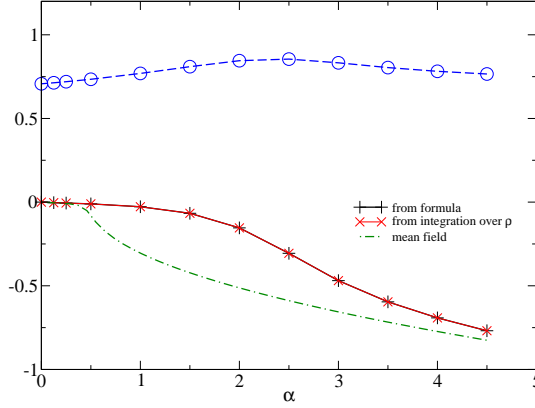


**Figure 11.** The average oscillator displacement  $\langle \hat{x} \rangle/x_0$  (full curve) as a function of  $\alpha$  for the case  $U = 0$ ,  $\varepsilon_f/\pi\Delta = -0.01$ ,  $\omega_0 = 0.6$ . The values calculated from the average over  $\rho(x)$  are indicated by crosses and those deduced from equation (14) by plus signs. The dashed-dot curve gives the corresponding mean field results. Also shown are the results of the root mean square deviation  $\Delta x/x_0$  (dashed curve and circles).

In this case, except for the small values of  $\alpha$ , there is quite a discrepancy between the exact and mean field results. The corresponding results for the root mean square deviation  $\Delta x$  are also shown. The results for this quantity are very similar to those shown in Fig. 9.

We can also examine the dependence of  $\rho(x)$  on the oscillator frequency  $\omega_0$ . In Fig. 12 we show the change in form of  $\rho(x)$  as the frequency is increased for a fixed value of  $\lambda$  in the strong coupling regime corresponding to  $\alpha = 4.5$  ( $U = 0$ ,  $\varepsilon_f = 0$ ).

We argued earlier that the minimum in the effective potential in the strong coupling regime occurs at a value of  $x \sim \sqrt{\lambda}/\omega_0$ . We would expect the peak in  $\rho(x)$  to behave in a similar way, so for fixed  $\lambda$  the peak positions should vary as  $1/\omega_0$ . This can be seen to be well satisfied in the results shown in Fig. 12. In the limit  $\omega_0 \rightarrow \infty$  the double peak feature disappears entirely and  $\rho(x)$  becomes a delta function at  $x = 0$ . In this limit the mean field equation for  $n_f$  still has a broken symmetry solution for  $\alpha > 0.5$ . This coincides with the static mean field solution for the Anderson model with  $U = -\lambda$ , if one first performs a Hubbard-Stratonovich transformation to couple the auxiliary field  $x(\tau)$  solely to the impurity charge. It differs by a factor of 2 from the mean field theory of the Anderson model with  $U = -\lambda$ , where the interaction term  $U n_{d,\uparrow} n_{d,\downarrow}$  is approximated by  $U(n_{d,\uparrow} \langle n_{d,\downarrow} \rangle + n_{d,\downarrow} \langle n_{d,\uparrow} \rangle - \langle n_{d,\uparrow} \rangle \langle n_{d,\downarrow} \rangle)$ .

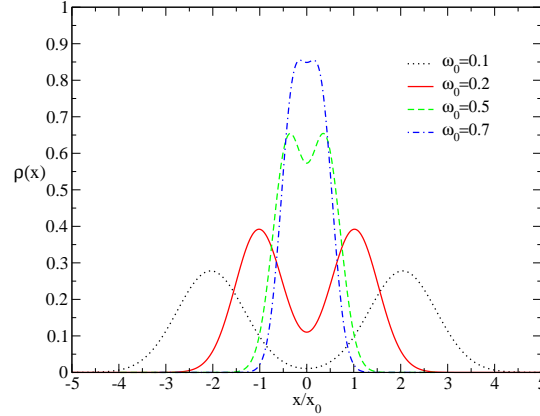


**Figure 12.** The variation of  $\rho(x)$  with the frequency  $\omega_0$  in the strong coupling case with  $\alpha = 4.5$ . The value of  $x_0$  is fixed and corresponds to  $1/\sqrt{\omega_0}$  for  $\omega_0 = 0.1$ .

### 3. Local Fluctuations in the Holstein-Hubbard Model

The states of broken symmetry predicted by the semiclassical/mean field theory for larger values of  $\lambda$  cannot exist for the impurity Anderson-Holstein model; the symmetry has to be restored in the exact solution. Symmetry breaking, however, as a result of a phase transition can occur in a lattice model. To study  $\rho(x)$  in the neighbourhood of a phase transition we consider the Holstein-Hubbard model, described by the Hamiltonian,

$$H = \sum_{i,j,\sigma} (t_{ij} c_{i,\sigma}^\dagger c_{j,\sigma} + \text{h.c.}) + U \sum_i \hat{n}_{i,\uparrow} \hat{n}_{i,\downarrow} \quad (15)$$

$$+ \omega_0 \sum_i b_i^\dagger b_i + g \sum_i (b_i + b_i^\dagger) \left( \sum_\sigma \hat{n}_{i,\sigma} - 1 \right).$$

$c_{i,\sigma}^\dagger$  creates an electron at lattice site  $i$  with spin  $\sigma$ , and  $b_i^\dagger$  a phonon with oscillator frequency  $\omega_0$ ,  $\hat{n}_{i,\sigma} = c_{i,\sigma}^\dagger c_{i,\sigma}$ . There is a coupling  $g$  to the local charge at each site, as in the Holstein model, and an on-site interaction  $U$  between spin-up and spin-down electrons, as in the Hubbard model. The hopping term  $t_{ij}$  between orbitals localised on each site leads to a conduction band with a density of states  $D_0(\omega)$  when  $g = U = 0$ . In the limit of infinite dimensions the model can be mapped into an effective Anderson-Holstein model, which can then be solved using the NRG. This has been described fully elsewhere [3, 2], and is known as the dynamical mean field theory (DMFT). For three dimensional systems, the mapping is only approximate. This approach is non-perturbative and can be applied in the strong interaction regime of these models to describe strong correlation effects, and indications are that it constitutes a good approximation when the self-energy of the electrons is local and a function of frequency only.

There have been several applications of the DMFT method to study phase transitions in the Hubbard-Holstein model [12, 13, 14, 15]. There are various possible transitions to states of broken symmetry in this model; bipolaronic (BP), charge ordered (CO), antiferromagnetic (AFM) and the superconducting (SC) state. We restrict our

attention here to the case of half-filling, so we do not include the superconducting case, which exists as a stable state away from half-filling. The transition first studied by the DMFT-NRG method for this model did not include the possibility of either charge order or antiferromagnetism [13, 14]. There is, however, a metal-insulator transition from the normal state (N) to the bipolaronic state (BP), first studied for the model with  $U = 0$ , which occurs as the electron-phonon coupling  $\lambda$  is increased at a critical value  $\lambda_c$ . The transition also occurs in the model with  $U \neq 0$ , at larger values of  $\lambda_c$ , as the attractive term induced by  $\lambda$  has to overcome the repulsion due to  $U(> 0)$ . If the possibility of transitions to charge order (CO) and antiferromagnetism are included, then it has been found that antiferromagnetism occurs for  $U - \lambda > 0$  and charge order for  $U - \lambda < 0$  [16, 17].

For the DMFT-NRG calculations presented here we have taken a Bethe lattice form for the density of states  $D_0(\omega)$  of the conduction electrons,

$$D_0(\omega) = \frac{1}{2\pi t^2} \sqrt{4t^2 - \omega^2}. \quad (16)$$

We choose a value  $t = 1$  to set the energy scale in the following, which corresponds to a bandwidth  $W = 4t = 4$ . The physically relevant regime in the lattice case is for phonon frequencies small compared with the bandwidth. In most of the calculations in this section we take  $\omega_0 = 0.6$ , which is small compared with the bandwidth of  $W$  but well away from the adiabatic limit. The distribution function for the local oscillator displacement  $\rho(x)$  was calculated from the DMFT-NRG density matrix using equation (2).

### 3.1. Model without long range order

We consider first the results for the normal to bipolaronic transition, which are shown in Fig. 13 for  $U = 2$  (left panel) and  $U = 5$  (right panel) and different values of  $\lambda$ .

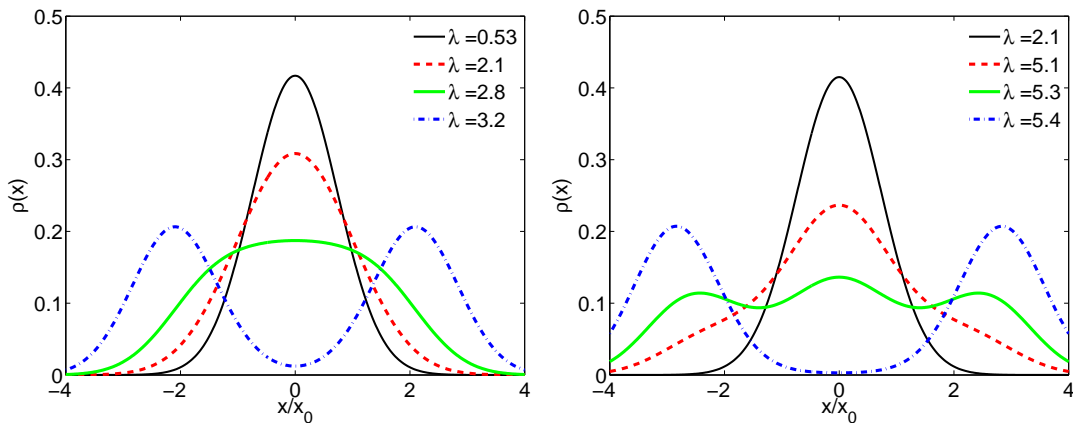


**Figure 13.** (Color online) The local probability distribution  $\rho(x)$  for  $U = 2$  (right part) for the N state and  $U = 5$  (left part) for various values of  $\lambda$  for  $\omega_0 = 0.6$ .

In the left panel we can see for the case of  $U = 2$  how the probability distribution becomes broader as  $\lambda$  is increased. As we do not allow for symmetry breaking here the system changes between zero occupation and double occupation with the associated oscillator fluctuations to minimise the energy. The situation is similar to the impurity case shown in Fig. 1, and a two peak form develops in a similar way. However in this case when the two peak structure develops a gap also appears in the electron density of states,  $D(\omega)$ , signaling the transition to an insulating bipolaronic state. The correlation can be seen in the corresponding results for  $D(\omega)$  shown in Fig. 14 over the transition regime.

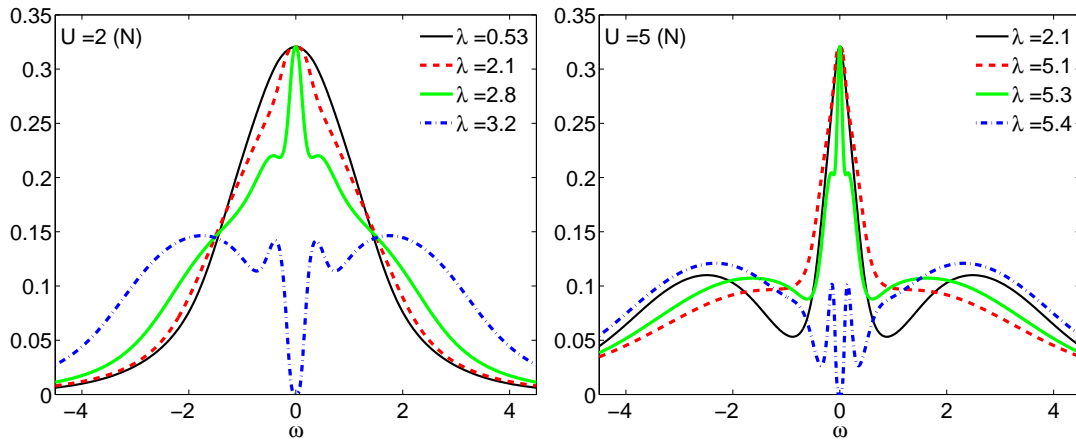


**Figure 14.** (Color online) The local electronic spectral functions  $D(\omega)$  in comparison for  $U = 2$  (left panel) and  $U = 5$  (right panel) for various  $\lambda$  and  $\omega_0 = 0.6$ .

This is in contrast to the impurity density of states shown in Fig. 3 where there is a shift of spectral weight from the region near  $\omega = 0$  to higher and lower values of  $\omega$ , but a narrow central peak at  $\omega = 0$  remains. The narrow peak reflects the fact that there is no broken symmetry in the impurity case, and there are fluctuations between the two potential wells that restore the symmetry. In the right panel the results for  $\rho(x)$  across the transition are shown for  $U = 5$ . There is a similar trend leading to a two peak structure in the bipolaronic phase, though at larger values of  $\lambda$  due to the larger value of  $U$ . However, in this case there is an intermediate regime where  $\rho(x)$  has three maxima, which is very close to the metal-bipolaron transition, and the change is more marked, occurring over smaller range of  $\lambda$ .

Similar as in the impurity case, Eq. (7), we can compute the effective potential  $V_{\text{eff}}(x)$ , which is formed locally in the lattice model due to the electron-phonon coupling, from the probability distribution. This is shown in Fig. 15 for the same values as before,  $U = 2$  (left panel) and  $U = 5$  (right panel).

In the case  $U = 2$  on increasing  $\lambda$  one sees that the potential becomes shallow and eventually develops two minima at finite  $\pm x_m$ . Note that although there are two minima already for  $\lambda = 2.8$ , fluctuations are sufficient to keep the system in a metallic state, as can be seen also from the spectral function in Fig. 14. When the minima are deeper,



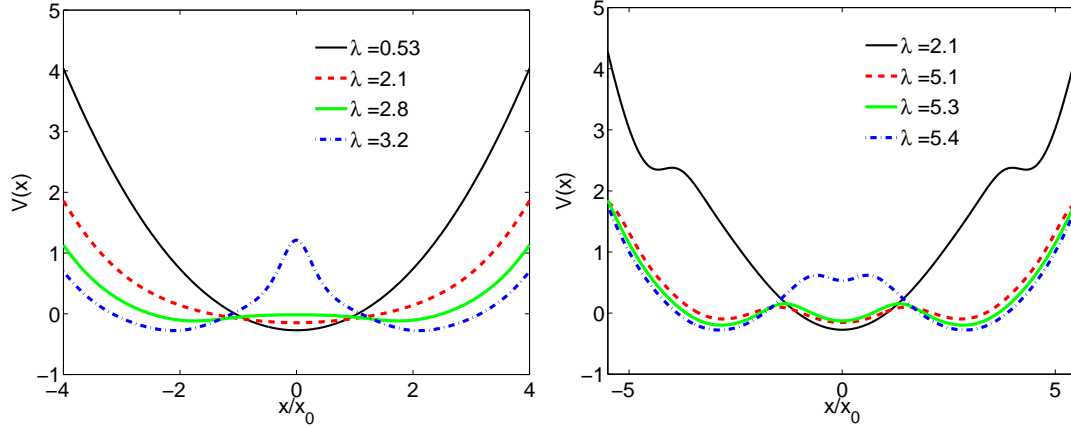


**Figure 15.** (Color online) The local effective potential  $V(x)$  for  $U = 2$  (left part) for the N state for  $U = 5$  (right part) for various values of  $\lambda$  for  $\omega_0 = 0.6$ .

as for  $\lambda = 3.2$ , the system is in the BP insulating state. The transition is continuous.

In the case  $U = 5$  the overall trend is similar, but larger values of  $\lambda$  are required to induce the transition. Close to the transition we can find a structure of 3 local minima, where the one at  $x = 0$  is lifted upon increasing  $\lambda$ . This is characteristic for a discontinuous transition which is expected to occur for larger values of  $U$  as discussed by Koller et al. [14].

If we restrict to the pure Holstein model ( $U = 0$ ), then it is also of interest here to study the quality of the semi-classical approximation. Similar as in the impurity case the potential can be calculated and one finds

$$V_{\text{s-cl}}(x) = -\frac{2}{3}D_0(\bar{\mu}(x))^3 - \bar{\mu}(x)^2 D_0(\bar{\mu}(x)) - \frac{2\bar{\mu}(x)}{\pi} \arcsin\left(\frac{\bar{\mu}(x)}{D}\right) + \frac{1}{2}\omega_0^2 x^2 - \mu, \quad (17)$$

where  $\bar{\mu}(x) = \mu - \sqrt{2\omega_0}gx$ . The condition  $\frac{\partial V_{\text{s-cl}}(x)}{\partial x} = 0$  gives the mean field solutions and one can infer that at half filling,  $\mu = 0$ , the potential has two minima if  $\lambda > \lambda_c^{\text{mf}} = \pi D/4$ . The value for this to occur in the DMFT with local quantum fluctuations is larger and also depends on  $\omega_0$ . For  $D = 2$  one has, e.g., for  $\omega_0 = 0.2$  the value  $\lambda_c \simeq 1.75$  and for  $\omega_0 = 0.6$  the value  $\lambda_c \simeq 2$ . For the first case,  $\omega_0 = 0.2$ , we give a comparison of the effective potential obtained in DMFT calculations and the semiclassical approximation (17) in Fig. 16 for two values of  $\lambda$ .

For the smaller value of  $\lambda$  with the minimum at  $x = 0$  one finds a quite good agreement between the calculations. However, closer to the transition the results vary significantly.  $\lambda = 1.6$  is still a metallic solution with a narrow quasiparticle peak in DMFT. As  $\lambda > \lambda_c^{\text{mf}}$  the semiclassical approximation possesses two shallow minima for this case which can barely be resolved on the plot. The positions (1.16 semi-classical, 2.32 DMFT-NRG) differ significantly from the DMFT result, where fluctuations keep the state metallic. Better agreement between for the position of the minima in the semiclassical approximation and DMFT can again found in the insulating (BP) phase.

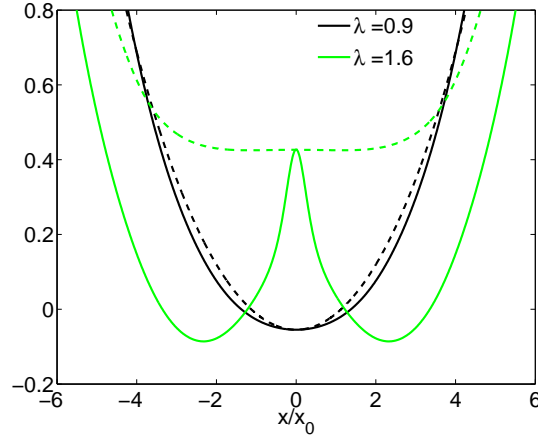


**Figure 16.** (Color online) Comparison of  $V(x)$  for DMFT-NRG calculation (full line) with the semi-classical approximation (dashed line) for  $\omega_0 = 0.2$ . The values of  $V_{s-cl}(x)$  have been offset to make the comparison clearer.

### 3.2. Model with long range order

To consider charge ordered states, the lattice is divided into two sublattices denoted by  $A$  and  $B$ . Charge order develops when the occupation values  $\langle \hat{n}_{i,A} \rangle \neq \langle \hat{n}_{i,B} \rangle$ , and their difference divided by 2 can be taken as the order parameter  $\Phi_{co}$ . As  $\langle \hat{n}_{i,A} + \hat{n}_{i,B} \rangle = 2$  at half filling,  $\Phi_{co}$  can be taken as  $1/2(\langle \hat{n}_{i,A} \rangle - 1)$ . When charge order occurs  $\rho(x)$  shifts position to a displaced state appropriate to the local charge to minimise the energy. This can be seen in Fig. 17 (left panel) where we show  $\rho(x)$  for  $U = 2$  and values of  $\lambda$  as charge order develops for  $\lambda > U$ .

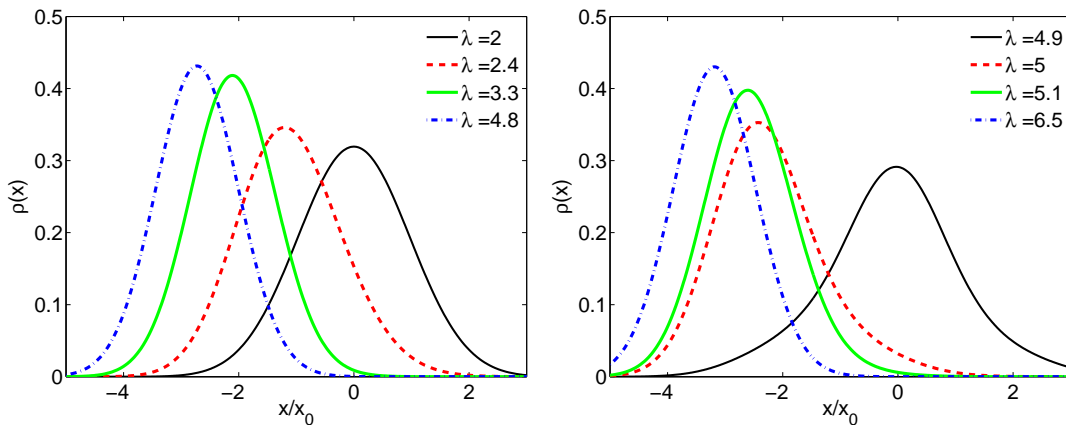


**Figure 17.** (Color online) The local probability distribution  $\rho(x)$  for  $U = 2$  (left part) for the CO state for  $U = 5$  (right part) for various values of  $\lambda$  for  $\omega_0 = 0.6$ .

In this case  $\rho(x)$  has a single peak which shifts and narrows slightly as  $\lambda$  is increased. The same trend can be seen in the right panel of Fig. 17 for the case  $U = 5$ , though the shifting and narrowing occurs more rapidly as  $\lambda$  is increased. The shifting of a single

peak with increasing  $\lambda$  is similar to the asymmetric impurity case shown in Fig. 7, though the narrowing is an extra feature.

The exact relation in equation (14) we derived earlier between the average displacement and the expectation value for occupation of the impurity site also holds for the lattice model. If we let  $\langle \hat{x} \rangle$  denote the value of  $\langle \hat{x}_{i,A} \rangle$ , then we have from equation (14)

$$\Phi_{\text{co}} = -\frac{\omega_0 \langle \hat{x} \rangle}{2\sqrt{\lambda}}, \quad (18)$$

so that the order parameter is directly proportional to  $\langle \hat{x} \rangle$ . Again we can test this relation by calculating  $\langle \hat{x} \rangle$  from the average over  $\rho(x)$  and use the NRG results for  $\Phi_{\text{co}}$ , and find that it is satisfied very precisely.

In Fig. 18 we plot  $\langle \hat{x} \rangle / x_0$  for various values of  $U$  as a function of  $\lambda$ , which from equation (18) is proportional to the order parameter  $\Phi_{\text{co}}$ .

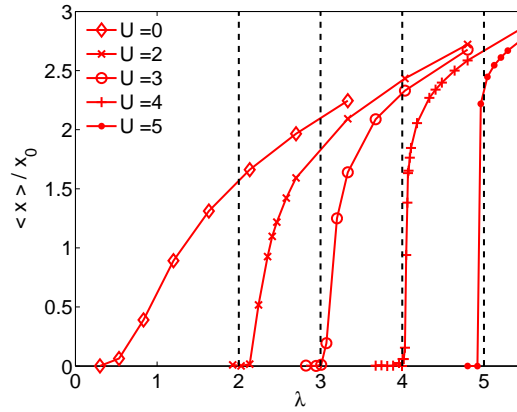


**Figure 18.** (Color online) The expectation values  $\langle x \rangle$  for various values of  $U$  as a function of  $\lambda$  for  $\omega_0 = 0.6$  in the CO state.

In the normal or antiferromagnetic state  $\langle \hat{x} \rangle = 0$ , and the onset of the charge order can be seen clearly to occur for  $\lambda \sim U$ . The transition increases sharply with increasing  $U$ , such that for  $U = 5$  it is discontinuous. There is a similar trend in the impurity case shown in Fig. 6, but it is more marked in the lattice case.

The mean square deviation  $(\Delta x)^2$  for the lattice coordinate, which can be deduced from the appropriate averages over  $\rho(x)$ , is a measure of the fluctuations of the order parameter. In Fig. 19  $(\Delta x)^2 / x_0^2$  is plotted for the same set of parameters as for  $\langle \hat{x} \rangle$ . This quantity is finite in the antiferromagnetic phase for  $\lambda < U$ , and increases significantly as the transition is approached. The fluctuations can be seen to become much greater in the region of the transition for the intermediate values of  $U$ , most prominently near the point  $U = \lambda = 4$ , where the transition changes from second to first order. This is a reflection of the fact that  $\rho(x)$  broadens at the transition and then narrows as  $\lambda$  is increased further. Once the charge order has been well established the fluctuations then fall off rapidly to give  $(\Delta x)^2 / x_0^2 = 1/2$ . Though the values of  $(\Delta x)^2$  away from the transition behave like the impurity case shown in Fig. 9, there is a very

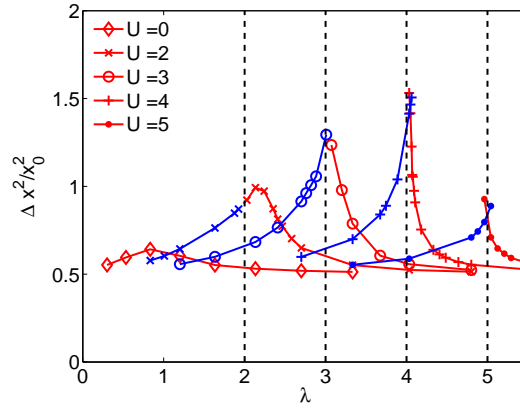


**Figure 19.** (Color online) The expectation values  $\Delta x^2$  for various values of  $U$  as a function of  $\lambda$  for  $\omega_0 = 0.6$  in the AFM state for  $\lambda < U$  and in the CO state for  $\lambda > U$ .

marked difference in the critical region especially for large  $U$ . An analysis of the effective potential is also possible for the CO case, but will be omitted here. For  $U = 0$  one can similarly derive a semiclassical potential. A detailed DMFT study of CO order in the Holstein model in the adiabatic limit, where also the probability distribution and the effective potential are discussed, has been given by Ciuchi et al. [18].

#### 4. Conclusions

We have shown how the reduced density matrix obtained from NRG calculations can provide physically relevant information about the local fluctuations. We have illustrated this by calculating the probability density function  $\rho(x)$  for the spatial coordinate  $x$  of the local oscillator in the impurity Anderson-Holstein and lattice Hubbard-Holstein models. This has enabled us to address a number of interesting questions. We have been able to see how the features in  $\rho(x)$  correlate with the features seen in the spectral density of the electrons as the interaction strength is increased. We have also deduced an effective potential  $V_{\text{eff}}(x)$ , such that the wavefunction  $|\psi(x)|^2$  of the Schrödinger equation corresponds to  $\rho(x)$ . This has enabled us to compare this potential with the one obtained from a semiclassical approximation, where the  $x$ -coordinate is treated as a classical variable, which is equivalent to the Born-Oppenheimer approximation. The results have provided a guide as to when the semiclassical approximation can be expected to give reliable results, and to clarify its limitations.

We have also been able to compare the fluctuations of  $x$  in the impurity case with those in the lattice model in the various parameter regimes. For the normal state BP insulator transition we found a double well potential for weaker coupling and a structure with three local minima for stronger coupling. The semiclassical approach only gave a good description for weaker electron-phonon coupling. Allowing for the symmetry breaking in the lattice model, we have found that  $\rho(x)$  broadens in the critical region of the antiferromagnetic to charge order phase transition. The critical fluctuations become

particularly marked in the intermediate  $U$  regime near the point where the ground state transition changes from continuous to discontinuous behaviour.

From a calculation of the reduced density matrix it is also possible to learn something about the local electronic fluctuations. If in equation (2) we integrate over the oscillator coordinate  $x$ , but do not carry out the sum over  $q$  and  $m_z$ , then we have components  $\rho(q, m_z)$  of the impurity reduced density matrix. From these, for example, we can deduce directly the impurity charge fluctuation,  $(\Delta\hat{n}_f)^2 = \langle(\hat{n}_f - \langle\hat{n}_f\rangle)^2\rangle$ ,

$$(\Delta\hat{n}_f)^2 = 4\rho(2, 0) + \sum_{m_z=\pm 1/2} \rho(0, m_z) - \left(2\rho(2, 0) + \sum_{m_z=\pm 1/2} \rho(0, m_z)\right)^2. \quad (19)$$

If the calculation of the reduced density matrix were to be terminated earlier, say at the neighbouring site to the impurity, local electronic fluctuations and near neighbour correlation functions could be deduced in a similar way.

## Acknowledgement

We thank Winfried Koller for his work in initiating this investigation and for his contribution with Dietrich Meyer to the development of the NRG programs.

- [1] K. Wilson, Rev. Mod. Phys. **47**, 773 (1975).
- [2] R. Bulla, T. Costi, and T. Pruschke, Rev. Mod. Phys. **80**, 395 (2008).
- [3] A. Georges, G. Kotliar, W. Krauth, and M. Rozenberg, Rev. Mod. Phys. **68**, 13 (1996).
- [4] P. W. Anderson, Phys. Rev. **124**, 41 (1961).
- [5] T. Holstein, Ann. Phys. (N.Y.) **8**, 325 (1959).
- [6] A. C. Hewson and D. Meyer, J. Phys.: Cond. Mat. **14**, 427 (2002).
- [7] P. S. Cornaglia, H. Ness, and D. R. Grempel, Phys. Rev. Lett. **93**, 147201 (2004).
- [8] W. Hofstetter, Phys. Rev. Lett. **85**, 1508 (2000).
- [9] R. Peters, T. Pruschke, and F. B. Anders, Phys. Rev. B **74**, 245114 (2006).
- [10] A. Weichselbaum and J. von Delft, Phys. Rev. Lett. **99**, 076402 (2007).
- [11] A. C. Hewson, J. Bauer, and W. Koller, Phys. Rev. B **73**, 045117 (2006).
- [12] P. Benedetti and R. Zeyher, Phys. Rev. B **58**, 14320 (1998).
- [13] D. Meyer, A. Hewson, and R. Bulla, Phys. Rev. Lett. **89**, 196401 (2002).
- [14] W. Koller, D. Meyer, and A. C. Hewson, Phys. Rev. B **70**, 155103 (2004).
- [15] W. Koller, A. C. Hewson, and D. M. Edwards, Phys. Rev. Lett. **95**, 256401 (2005).
- [16] J. Bauer, cond-mat/0907.3751 (unpublished).
- [17] J. Bauer and A. C. Hewson, to be published (unpublished).
- [18] S. Ciuchi and F. de Pasquale, Phys. Rev. B **59**, 5431 (1999).